Crystallographic Studies of the Catalytic and a Second Site in Fumarase C from *Escherichia coli*[†,‡]

Todd Weaver and Leonard Banaszak*

Department of Biochemistry, University of Minnesota, Minneapolis, Minnesota 55455

Received June 20, 1996; Revised Manuscript Received August 19, 1996[⊗]

ABSTRACT: Fumarase C catalyzes the stereospecific interconversion of fumarate to L-malate as part of the metabolic citric acid or Kreb's cycle. The recent three-dimensional structure of fumarase C from *Escherichia coli* has identified a binding site for anions which is generated by side chains from three of the four subunits within the tetramer (Weaver *et al.*, 1995). These same side chains are found in the three most highly conserved regions within the class II fumarase superfamily. The site was initially characterized by crystallographic studies through the binding of a heavy atom derivative, tungstate. A number of additional crystallographic structures using fumarase crystals with bound inhibitors and poor substrates have now been studied. The new structures have both confirmed the originally proposed active site, site A, and led to the discovery of a novel second binding site that is structurally nearby, site B. Site A utilizes a combination of residues, including H188, T187, K324, N326, T100, N141, S139, and S140, to form direct hydrogen bonds to each of the inhibitors. The A-site has been demonstrated by studying crystalline fumarase with the bound competitive inhibitors—citrate and 1,2,4,5-benzenetetracarboxylic acid. The crystal structure of fumarase C with β-(trimethylsilyl)maleate, a *cis* substrate for fumarase, has led to the discovery of the second site or B-site. Sites A and B have different properties in terms of their three-dimensional structures. Site B, for example, is formed by atoms from only one of the subunits within the tetramer and mainly by atoms from a π-helix between residues H129 through N135. The crystal structures show that the two locations are separated by ∼12 Å. A highly coordinated buried water molecule is also found at the active or A-site. The high-resolution crystal structures describe both sites, and atoms near the A-site are used to propose a likely enzyme/substrate complex.

Fumarase catalyzes the reversible, stereospecific hydration/dehydration of fumarate to L-malate during the operation of the ubiquitous Kreb's cycle. The K_{eq} for the reaction is 4.4 at 25 °C in the direction of L-malate formation (Hill & Teipel, 1971). Fumarases can be divided into class I and class II types, both of which are found within *Escherichia coli* (Guest *et al.*, 1985). Class I fumarases are heat labile, iron dependent, 4Fe-4S cluster containing, dimeric proteins of 120 kDa. Fumarase A and fumarase B are examples of the class I form and share 90% sequence identity (Woods *et al.*, 1988). To date, there is no crystal structure for a class I fumarase.

Fumarase C is a member of the class II enzymes. From *E. coli*, it is a tetramer with each polypeptide chain consisting of 467 amino acids and no known metal ion requirement. The expression of fumarase C supplies *E. coli* with a form of the enzyme devoid of the unstable 4Fe-4S clusters found within fumarase A and B. Because of the presence of two different classes of enzymes, *E. coli* can adapt to unfavorable oxygen tensions by inducing the O_2 stable form—fumarase C (Greenberg *et al.*, 1990; Liochev & Fridovich, 1992).

The class II fumarases belong to a family of proteins that includes aspartase, adenylosuccinate lyase, arginosuccinate lyase, and δ-crystallin. The amino acid sequence identity between aspartase and fumarase C is 38% (Woods *et al.*, 1986). Three regions which have even higher levels of identity have been identified (Simpson *et al.*, 1994). The three regions are 129−146, 181−200, and 312−331, based on the numbering from fumarase C. In the crystal structure of the tetramer of fumarase C, the three segments, one from each of three subunits, come together in a unique region thought to be the active site (Weaver *et al.*, 1995). A sequence alignment of 22 family members has further confirmed the high identity within these three regions. In fact, G317, S318, S319, P322, K324, and N326 are some of the invariant residues among all family members.

The catalytic reaction in the direction of fumarate formation from L-malate is shown in Figure 1. The removal of a water molecule from L-malate generates the olefinic compound—fumarate. However, the water is removed in two steps—first in the form of a proton and then the remainder as an OH^- ion. This is an important consideration because it is believed that two different basic groups are necessary for the catalytic reaction (Brandt *et al.*, 1963). These two sites are labeled B_1 and B_2 in Figure 1. One of the basic groups, B_1 in Figure 1, has a p*K* which was not temperature dependent and is therefore thought to be a −COOH. The other had a ΔH of ionization similar to an imidazole side chain (Brandt *et al.*, 1963).

In terms of the basic groups B_1 and B_2, the enzyme with B_1 protonated is not in the correct state for the reaction to begin in the direction of fumarate production. The proton from B_1 must first leave and then the substrate, L-malate, M in Figure 1, can bind. B_1 then becomes the acceptor site

[†] Supported by a grant from the National Science Foundation, MCB 9318699.

[‡] The coordinates for the crystal structures of the three forms of protein described in the accompanying text have been deposited in the Brookhaven Protein Data Bank with the accession codes 1FUO, 1FUP, and 1FUQ.

* To whom correspondence should be addressed. Telephone: 612-626-6597. Fax: 612-625-2163. Email: len_b@dccc.med.umn.edu.

[⊗] Abstract published in *Advance ACS Abstracts,* October 15, 1996.

S0006-2960(96)01470-5 CCC: $12.00

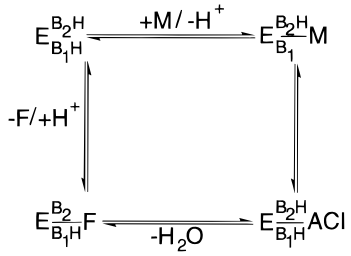

FIGURE 1: Proposed catalytic reaction scheme for fumarase C. The dehydratase reaction is thought to proceed through the *aci*-carboxylate intermediate (ACI) depicted above. M represents L-malate, F represents fumarate, and ACI represents the *aci*-carboxylate intermediate. In the direction of fumarate production and from the top left of the figure, the initial step in the reaction is binding of L-malate (M). This causes a displacement of the proton from base 1 (B_1H) remaining from the previous catalytic cycle. The initial step in the reaction mechanism is thought to be the removal of the C3 proton to the acceptor site B_1, thereby generating an unstable carbanion. Formation of the *aci*-carboxylate intermediate (ACI) stabilizes the carbanion radical and leaves the enzyme in the doubly protonated state. Rearrangement of the *aci*-carboxylate intermediate along with proton donation from the second catalytic base (B_2H) leads to the removal of the hydroxyl group from the C2 position in the form of H_2O. As mentioned in the text, the last product off is the "sticky" proton removed during the first catalytic step. The removal of the sticky proton may be facilitated by L-malate binding. In this manner, L-malate prevents itself from being trapped in a dead-end complex with the doubly protonated state of fumarase.

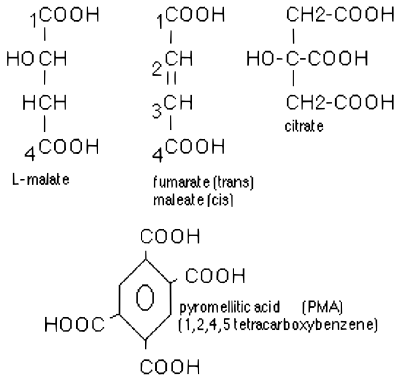

FIGURE 2: L-Malate and fumarate. The chemical structures of L-malate, fumarate, maleate, citrate, and pyromellitic acid are shown. Depending on a *trans* versus *cis* configuration around C3−C4, the dicarboxylic acids are fumarate and maleate, respectively. *β*-(Trimethylsilyl)maleate occurs when the C3 hydrogen of maleate is replaced by $(CH_3)_3Si-$.

for the first step in the catalytic reaction—proton removal. A carbanion is formed following proton abstraction from the C3 position of L-malate by B_1 and is stabilized by a resonance form—the *aci*-carboxylate intermediate labeled "ACI" in Figure 1 (Blanchard & Cleland, 1980; Rose *et al.*, 1992). Figure 2 contains the carbon numbering system for L-malate and fumarate.

At the point in the reaction profile of the *aci*-carboxylate intermediate, both B_1 and B_2 are protonated. The subsequent rearrangement of the *aci*-carboxylate intermediate and donation of a proton from the B_2-site on fumarase to the leaving OH^- group at the C2 position leads to the formation of a molecule of water. The "sticky" proton is left at the B_1 site. Its removal probably accompanies the binding of L-malate in the next reaction cycle (Rose *et al.*, 1992). In this manner, fumarase is prevented from being trapped in the dead-end complex $E-B_1H-M$. The $E-B_1H-M$ complex is unproductive because it is unable to accept any additional protons from the C3 position of L-malate during the next catalytic cycle. Apparently, the correct protonation state of the B_1 and B_2 sites is critical for the recycling of the fumarase reaction.

As noted above and in Figure 1, the H^+ and OH^-, which are products of the reaction in the direction of fumarate formation, probably do not enter or leave the enzyme as the same water molecule. In fact, the exchange rate between the C3 proton of malate, $E-B_1H$ in Figure 1, and solvent is slower than the ^{18}OH/malate exchange (Hansen *et al.*, 1969). The differing rates for product release have mechanistic implications which we have attempted to show by the presence of two forms of the enzyme labeled E−M and E−F in Figure 1. In terms of a second round of catalysis, one is thought to exist as an isoenzyme specific for L-malate (E−M in Figure 1) and the other for fumarate (E−F in Figure 1) (Rose *et al.*, 1992). Because the enzyme begins and ends the catalytic reaction with different states of the enzyme, others have labeled this an "isomechanism" (Rebholz & Northrup, 1994). The enzyme isomerization step in the reaction pathway has been attributed to a slow deprotonation/reprotonation of active site residues upon binding substrate (Rose *et al.*, 1993).

Isotope exchange studies at pH 7.3 have shown that a water molecule is the first product released, followed by fumarate, and then the proton derived from the C3 position (Hansen *et al.*, 1969). On the basis of the isotope effects and inhibition patterns with the *aci*-nitro anion radical of 3-nitro-2-hydroxypropionate, a mechanism has been proposed where the carboxylate group is responsible for removal of the C3 proton, thereby generating an unstable anion that is stabilized by the *aci*-carboxylate intermediate. The carbon−oxygen bond cleavage at the C2 position is concomitant with proton transfer from the imidazole group on fumarase, leaving water and fumarate (Blanchard & Cleland, 1980).

To further complicate studies of the structure/mechanism relationship, it has been shown that the reaction proceeds at higher than expected rates in the presence of high substrate concentration. At low substrate concentrations, fumarase exhibits Michaelis−Menten kinetics, where classic saturation curves are evident in the $[v_0]$ vs [S] plots. At substrate concentrations greater than five times K_m, fumarase exhibits substrate activation. At concentrations greater than 0.1 M, inhibition can occur (Hill & Teipel, 1971). A number of anions, some found in frequently used buffers, affect the activity of fumarase and thereby constitute a second subsite at or near the true catalytic site. The evidence for anions binding to the catalytic site or a nearby site dates back to the original papers describing fumarase activity (Alberty *et al.*, 1954; Alberty & Bock, 1953). Others have confirmed these observations (Keruchenko *et al.*, 1992).

The effects of substrate and other anions have been explained by several different mechanisms. One explanation is that substrate activation occurs because of the binding of an additional molecule to a second site—an apparent activator site [for a review see Hill and Teipel (1971)]. Another mechanism that fits the kinetic data was termed "negative cooperativity" (Hill & Teipel, 1971; Conway & Koshland, 1968). In this interpretation, fumarase possesses two or more identical binding sites for substrate that display cooperativity between themselves. The binding of the first substrate molecule decreases the affinity of substrate for the other sites. This seems unlikely in view of the crystal structures which

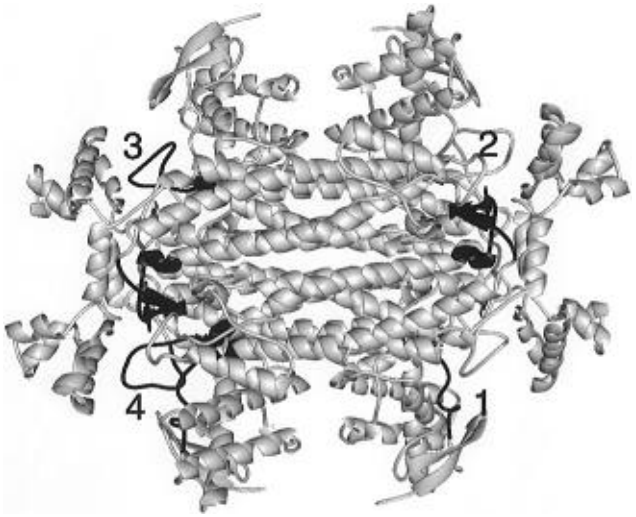

FIGURE 3: Fumarase C tetramer. Tetrameric fumarase is shown in cartoon form. A single subunit has an asymmetric appearance while the tetramer has a visible globular appearance. The core of the molecule consists of a bundle of 20 α-helices from the five-helix bundle of domain 2. The projections from the core of the tetramer are generated from domains 1 and 3 of each subunit. The blackened regions within the tetramer represent the three areas of highest sequence identity among the fumarase superfamily. The highly conserved segments include 129−145, 181−200, and 312−331. The approximate locations of the four active sites are marked by numbers 1 through 4. The site at the bottom left, active site 4, shows the necessary contributions from all three areas colored in black. This figure and Figures 4−7 were made with the program MIDAS (Ferrin *et al.*, 1988).

support the presence of an adjacent binding site in the vicinity of the active site.

The crystal structure of fumarase has been previously reported by Weaver *et al.* (1995) and has the four subunits arranged with 222 point symmetry as shown in Figure 3. Each monomer consists of three domains. The individual domains are generated in a sequential fashion. The second domain consists of a five-helix bundle. The core of the tetramer is a 20-helix bundle generated from domain 2 of each of the four monomers. The overall three-dimensional structure with the central core of helices is homologous to that of δ-crystallin (Simpson *et al.*, 1994).

As mentioned previously, the three regions of increased identity are believed to mark the location of the active site in fumarase. In the primary structure, the three regions include residues 129−146, 181−200, and 312−331 and have been highlighted in Figure 3. The three regions that share high sequence identity are spatially quite removed from one another in a single monomer (Weaver *et al.*, 1995). However, in the tetramer, the three segments are juxtaposed, generating the putative active site. Figure 3 has subunits B, C, and D colored black where all three conserved regions come together and form the active site, and this is represented by the number 4. In the initial X-ray crystallographic study, this location also marked the binding site for a tungstate ion, a reasonable phosphate analog, and a known competitive inhibitor of fumarase. This was the status of our understanding of the conformation at the completion of what we thought to be a study of the apoenzyme (Weaver *et al.*, 1995).

In this next stage of the investigation, we have tried to define the structural details around the fumarase active site. There are two general requirements for compounds to undergo fumarase catalysis. First, there must be two negatively charged carboxylate groups that will presumably interact with positive charges on the enzyme. Second, the hydroxyl groups in all substrates must have the same configuration as in L-malate. L-Malate derivatives that have substituents other than a hydrogen *erythro* to the hydroxyl group are not substrates for fumarase. With the above two criteria in mind, fumarase has been found to react with a number of nonnatural substrates (Hill & Teipel, 1971) such as fluoro-, chloro-, and bromofumarate, acetylene dicarboxylate, L-*threo*-chloromalate, L-tartrate, L-*trans*-2,3-epoxysuccinate, and β-(trimethylsilyl)maleate (TMSM).[1] Of all the listed nonnatural substrates above, only TMSM has a *cis* orientation about the carboxylate groups.

Not unexpectedly, similar criteria apply to inhibitors. There are a number of known inhibitors for fumarase: citrate, L-isocitrate, mesotartrate, dimethyl fumarate, *trans*-aconitate, succinate, maleate, mesaconitate, PMA, maleate, phosphate, tungstate, tripolyphosphate, adenosine triphosphate(ATP), (*S*)-2,3-dicarboxyaziridine, and 3-nitro-2-hydroxypropionate (Hill & Teipel, 1971). A representative sampling of substrates and inhibitors was shown in Figure 2. (*S*)-2,3-Dicarboxyaziridine and 3-nitro-2-hydroxypropionate are both proposed to be transition state analogs for fumarase (Greenhut et al., 1985; Porter & Bright, 1980).

In the text which follows, several refined X-ray structures are reported in which either an inhibitor or substrate analog has been soaked into the crystal before the diffraction data were collected. In three different inhibited forms of fumarase C from *E. coli*, ligands containing carboxylate groups have been identified at two unique sites. On the basis of previous biochemical evidence indicating a role for a second subsite remote from the active site, the studies described below may reveal both bound forms of the catalytic and activator sites.

EXPERIMENTAL PROCEDURES

Purification. Fumarase was purified from *E. coli* strain JM105 harboring the pFUMC001 plasmid encoding the native enzyme. This strain and another with a five-histidine C-terminal arm was a generous gift from Drs. M. Donnelly and P. Wilkens-Stevens of The Argonne National Laboratory. Although the original structure was reported with the histidine arm form, we have since used mainly the unmodified protein. We report below the purification scheme for the native recombinant enzyme.

The cells were grown to an optical density of 0.40−0.80 at 600 nm in 2.8 L Fernbach flasks containing 1.0 L of Luria broth, at which time they were induced with 1 mM IPTG for 4−6 h. The cells were harvested via centrifugation at 700*g* for 30 min and stored at −80 °C. Typically 4−6 g of *E. coli* was obtained per liter of media and up to 1−3 mg of purified fumarase was obtained from a wet weight gram of *E. coli*. The cells were suspended, 1 g/mL, into buffer A (50 mM Tris-HCl, pH 8.40, 10 mM EDTA, 2 mM DTT) and disrupted via sonication for 3 × 3 min pulses while being stirred in an 2-propanol/dry ice bath. The temperature of the cell extract was maintained below 10 °C. Upon cell lysis, the cellular debris was removed by centrifugation at 25000*g* for 45 min. Enzyme activity was measured by an assay which followed fumarate production spectrophotometrically at 250 nm (Weaver *et al.*, 1993).

[1] Abbreviations: PMA, 1,2,4,5-benzenetetracarboxylic acid or pyromellitic acid; TMSM, β-(trimethylsilyl)maleate.

Table 1: Data Collection and Processing Statistics

data set	resolution (Å)	unique reflections	% completeness	R_{merge}	$\langle I/\sigma(I)\rangle$	redundancy
native	1.98	69760	93.5	6.20	10.28	4.45
PMA[a]	2.3	44413	98.5	7.32	7.92	6.34
WO_4[a]	2.0	68527	94.8	6.92	9.01	5.39
TMSM[a]	2.0	66809	94.2	7.78	8.59	4.04

[a] All derivatives were soaked in solutions containing the ligand at 100 mM concentrations overnight (10−14 h). PMA is 1,2,4,5-benzenetetracarboxylate; TMSM is β-(trimethylsilyl)maleate.

With four exceptions, the remaining steps in the purification are identical to those previously reported (Weaver *et al.*, 1993). The exceptions were that a 600 mL G25-80 gel filtration column equilibrated in buffer B (15 mM Tris-HCl, pH 8.40, 5 mM EDTA, 2 mM DTT) was used for desalting the initial extract and the pooled fractions after the ion-exchange (Q-Sepharose) column. Neither the phenyl-Sepharose nor the red A columns were employed (Weaver *et al.*, 1993).

Crystallization. The crystallization of fumarase from *E. coli* has been previously described (Weaver *et al.*, 1993). The crystals were of the $C222_1$ habit with cell dimensions of $a = 104.0$ Å, $b = 219.9$ Å, $c = 86.7$ Å, and $\alpha = \beta = \gamma = 90°$. There are two subunits per asymmetric unit. Crystal dimensions were typically 1.0 mm × 0.5 mm × 0.4 mm. Crystals were grown by the hanging-drop method out of a solution of 300 mM citrate, pH 6.0, and 14% PEG 4000.

Inhibitor Complex Formation in the Crystalline State. Native fumarase crystals were transferred to 1 mL vials containing 300 mL of artificial mother liquor which included 150 mM citrate, pH 6.0, and 14% PEG 4000. Each inhibitor was dissolved into the artificial mother liquor, and the resulting solution was adjusted to pH 6.0. The appropriate volume of inhibitor was added to the crystal-containing vials to obtain a final concentration of 100 mM. All trials were allowed to soak overnight (10−14 h).

The following compounds were soaked into crystals and a complete set of X-ray diffraction data was collected: PMA, sodium tungstate, bromo- and chlorofumarate, 3-nitro 2-hydroxypropionate, *trans*-aconitate, ATP, citraconitic acid, mesotartrate, and TMSM. Representative structures for some of these compounds are given in Figure 2. No further soak conditions were needed for generation of the citrate and L-malate binding sites as they are present in the "native" crystals. Although there is chemical evidence for all of these compounds binding to fumarase, analyses of the X-ray results proved that only in a few cases was the citrate replaced. It is unclear why more of the inhibitors did not replace the bound citrate. The pH of crystal growth, strength of citrate binding, and proposed isomechanistic forms of fumarase may lead to an explanation.

Data Collection and Processing. All data sets were collected at room temperature using a Siemens-Nicollet area detector and a monochromatic source from a graphite crystal giving Cu Kα radiation ($\lambda = 1.542$ Å). The X-rays were generated by a rotating anode operating at 45 kV and 200 mA. One crystal was utilized for each data set, and data reduction was carried out with the XENGEN package of programs (Howard *et al.*, 1987). Details and statistics of the X-ray diffraction data sets are described in Table 1. The crystals are generally of excellent quality, which was demonstrated by a good R_{merge} value. As can be seen in Table 1, the resolution varies between 2.0 and 2.3 Å. All derivatives were first examined utilizing $|F_o|_d - |F_o|_n$, $2|F_o| - |F_c|$, and $|F_o| - |F_c|$ electron density maps. $|F_o|_d$ and $|F_o|_n$ are the observed structure amplitudes from the soaked and native crystals, respectively. Those compounds that gave virtually flat difference maps were assumed to not contain any bound ligand. PMA and tungstate gave large $|F_o|_d - |F_o|_n$ difference peaks at the active site while TMSM gave interpretable electron density at the B-site, especially around the trimethylsilyl substituent.

Table 2: Refinement Statistics for Fumarase Inhibitor/Substrate Complexes

data set	native	PMA	TMSM
resolution (Å)	8.0−1.98	8.0−2.0	8.0−2.0
R_{free}	20.6	23.4	23.3
R_{factor}	16.5	18.5	18.7
no. of reflections $I/\sigma(I)$	63157	64254	63434
protein atoms	6914	6907	6914
water molecules	442	353	395
ligand atoms	42	52	50
rmsd lengths (Å)	0.007	0.006	0.007
rmsd angles (deg)	1.261	1.253	1.279
rmsd dihedrals (deg)	21.057	21.026	21.151
rmsd impropers (deg)	1.269	1.257	1.286

Refinement. A round of Powell minimization within X-PLOR (Brünger *et al.*, 1987) utilizing the coordinates described by Weaver *et al.* (1995) started the refinement for all of the derivative data sets utilizing the native, citrate-containing coordinates. Typically after the initial round of refinement, the R_{factor} was below 20.0% and the R_{free} was below 24%. A core of water molecules was included in the starting coordinates, and after the first round of refinement, the water molecules were reconfirmed through the use of electron density maps calculated with the coefficients $(2|F_o| - |F_c|, \alpha_c)$ and $(|F_o| - |F_c|, \alpha_c)$. α_c's are the phases based on the model coordinates.

Water molecules obeying proper hydrogen-bonding conditions with electron densities greater than 1.0σ on a $2|F_o| - |F_c|$ and 3.0σ on a $|F_o| - |F_c|$ map were included. The coordinates for the ligands were obtained from the Cambridge Small Molecule Databank using the program QUEST and converted from fractional to the orthogonal angstrom coordinate system. Atoms belonging to the ligands were added only after the reexamination of the water molecules and during the final stages of refinement. The ligand bond lengths and angles were tightly constrained once proper positioning into the electron density was obtained. All of the fitting and rebuilding was done with the program O (Jones *et al.*, 1991). After each stage of manual model rebuilding, 50 cycles of Powell minimization were carried out.

Table 2 summarizes the final refinement results for the fumarase inhibitor/substrate data sets which contained significant difference electron density. Note that both the R_{factor} and R_{free} are better than those normally associated with an asymmetric unit containing 900 amino acids. The rms deviations from canonical values for bond lengths and angles are acceptable. Last of all, Table 2 shows that each of the derivative models is of the same reliability, and the X-ray data have been measured to about 2 Å resolution.

RESULTS

Inhibitors and Substrates—Two Adjacent Sites. The crystallographic results discussed below will describe the presence of two adjacent binding sites in the fumarase complexes which have been studied. The two different locations have been labeled "site A" and "site B". Site A refers to the position of bound citrate. On the basis of the fact that citrate is a competitive inhibitor, it is the putative catalytic site. Site B is a short distance away and has been shown to bind malate and TMSM. Since L-malate has been suggested to be an activator as well as a substrate, we will refer to the B-site as the activator location. Conclusive evidence for site B being the activator site cannot be provided by this structural study. However, as will be shown below, the structural studies fit the suggestion that an activator subsite is near the location of the catalytic center.

Before the detailed conformational results are described, a brief overview of the complications added as a result of the discovery of two sites is as follows. As can be seen in Figure 2, all of the ligands studied in the crystalline state have in common at least one carboxylate group, and each has been implicated by chemical studies to bind at the active site of fumarase. TMSM, a poor *cis* substrate, should bind to the A-site (Biton, 1994). It, however, is found at the B-site. The active site or A-site generally contained bound citrate since the native protein was crystallized from buffers with very high concentrations of citrate. Only PMA competed successfully with citrate for the A-site. Last of all, in the X-ray maps of the native enzyme, we have found yet unreported electron density at the B-site. Chemical studies have so far been unsuccessful in identifying the compound. It has tentatively been identified as L-malate which may remain from the purification procedure.

Four different ligands within three crystalline complexes provide the data describing the two sites. Table 2 summarizes the refinement results where the complexes are listed as native, PMA, and TMSM. The R_{factor}, R_{free}, and resolution are excellent for all three crystal forms. In two of the three complexes (native and TMSM), citrate is bound to the A-site. Only in the PMA complex is the citrate replaced by this potent inhibitor. In the native and PMA forms, malate has been modeled at site B.

The two sites are shown in Figure 4. The proximity of the two binding sites to each other should be apparent. Two general points should be noted: site A or the active site has components from three of the four subunits comprising the tetramer; site B is formed by atoms from only one subunit, "b" in Figure 4. In addition to atoms belonging to the protein and ligands visible in Figure 4, near the citrate ligand is a single atom position which was interpreted as a solvent site and discussed in greater detail below.

The A-site or active site with bound citrate therefore has atoms involved in binding the inhibitor and a single water molecule. Essentially the same results were obtained at site A with PMA instead of citrate. A stereo diagram of bound PMA is shown in Figure 5. In broadest terms, the A-site has contributions from residues 96−100 and 139−141 of subunit B and residues 318−331 from subunit C, and subunit D adds residues 187 and 188. Two of the carboxylates of citrate and PMA are located in essentially the same place in the two different complexes. One of them interacts with K324, T187, and N326. The other carboxylate appears to be close to N326 and T100. H188 is between the two locations and is positioned in a manner such that it can interact with both of the aforementioned carboxylates. The specific hydrogen-bonding distances are given in Table 3, which also includes distances to protein atoms from the third carboxylate of citrate and the third and fourth carboxylate of PMA.

Table 3: Hydrogen Bond Distances to Ligands at the A-Site of Fumarase C

side chain/ water atom donor	citrate atom	distance (Å)[a]	PMA atom	distance (Å)[b]
His 188-NE2	citrate-O4	3.03		
Lys 324-NZ	citrate-O4	2.94	PMA-O4	3.40
Asn 326-ND2	citrate-O4, O2	3.10, 3.02	PMA-O4, O2	2.91, 3.41
Asn 141-ND2	citrate-O3	3.09	PMA-O3	3.25
Asn 135-ND2			PMA-O6	3.38
Ser 139-OG	citrate-O7	2.75	PMA-O7	2.37
Ser 140-N	citrate-O6, O7	3.66, 2.83	PMA-O6	2.58
Ser 140-OG	citrate-O6	2.85	PMA-O6	3.12
Thr 100-OG1	citrate-O1	2.94	PMA-O1	2.72
Thr 187-OG1	citrate-O4, O3	3.26, 3.09	PMA-O3	3.01

[a] Distances were determined using the refined crystallographic coordinates from native fumarase crystals. [b] Distances were determined using the refined crystallographic coordinates from the fumarase/PMA derivative.

There are two other notable points about the A-site. As can be seen from the view in Figure 5, E331c forms an ion pair with H188d which resembles the charge-relay system found in a number of other enzymes. In addition, at site A in both the native and PMA structures, a solvent molecule is found near the H188 and the bound inhibitor. The coordination of this solvent site will be described in more detail below.

The binding of residues S140b and N141b at the A-site is especially important as this region leads into the B-site generated by residues 126−132. The B-site has been characterized with two bound ligands—malate and TMSM. It is visible in Figure 4. The *cis* substrate, TMSM, was the first to be characterized. The 14 electrons associated with the silicon atom gave good difference electron density. In fact, the $|F_o|_d - |F_o|_n$ difference map for the TMSM derivative contained a 6σ peak at the site of the trimethylsilyl group. At this point, a careful reexamination of the native map showed that there was unaccounted for electron density at the same location. Because of its appearance, we believe this electron density to contain a bound molecule of L-malate. As noted above, L-malate was used to elute bound fumarase C from the pyromellitic acid affinity column.

As is apparent in Figure 4, the B-site is generated from a one-turn π-helix as determined by PROCHECK (Laskowski *et al.*, 1993). The π-helix begins with H129 and ends with N135. The amino acid sequence through this region is -H_{129}-P-N-D-D-V-N_{135}-. Main-chain hydrogen bonds from H129-O to V134-N, P130-O to N135-N, and N131-CO to K136-NH help to stabilize the π-helix. Further stabilization of this short helix is provided by ligand/main-chain and ligand/side-chain interactions as well as side-chain/main-chain interactions. The amino acid sequence through this short helix is highly conserved in the aspartases, but not among the other family members such as arginosuccinate lyase, adenylosuccinate lyase, 3-carboxy-*cis*,*cis*-muconate lactonizing enzyme, and δ-crystallin.

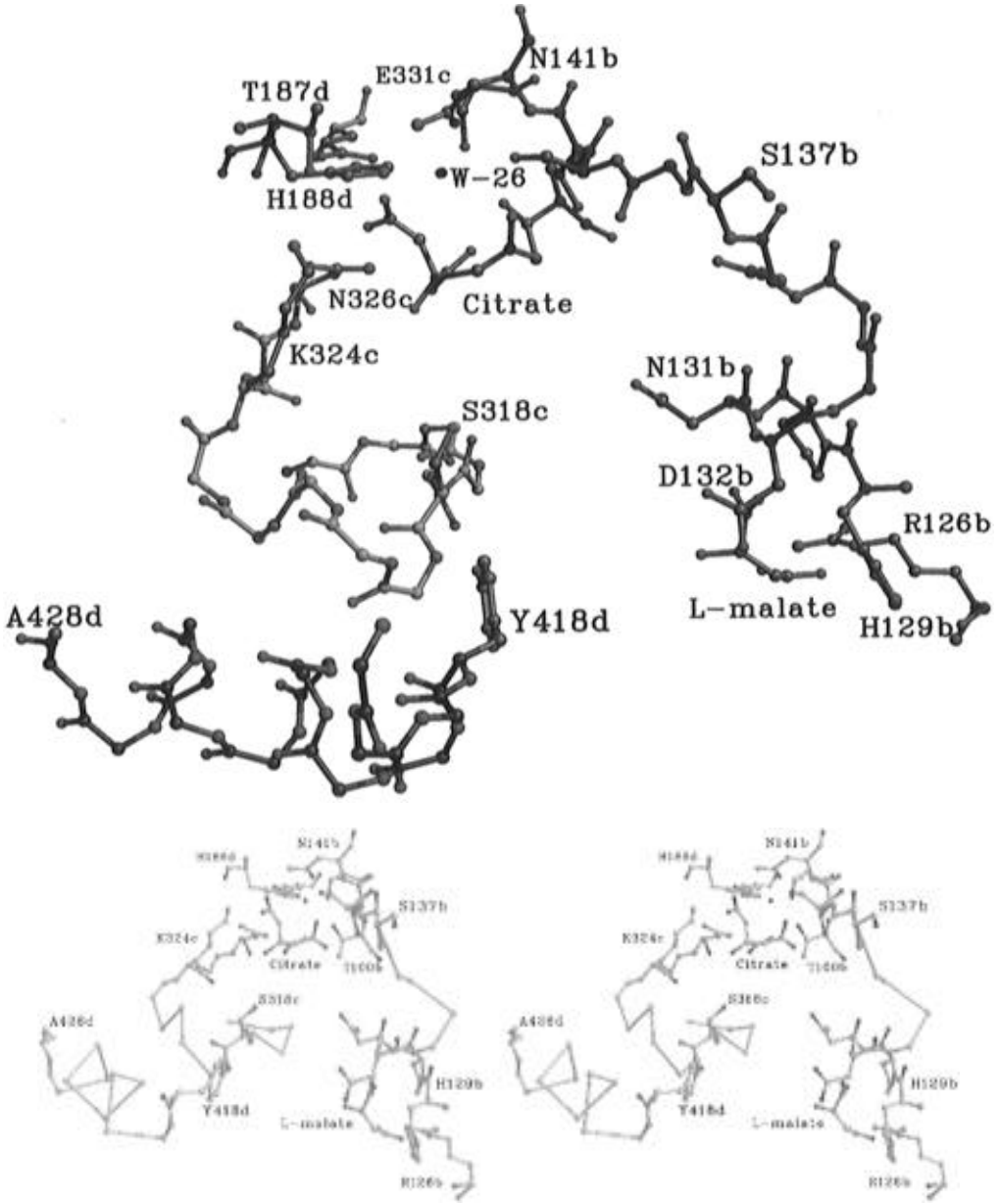

FIGURE 4: Multisubunit A- and B-site region of fumarase. The drawings show the steric relationship of the A- and B-sites in the native fumarase structure. In both (A, top) and (B, bottom), side chains are labeled with the appropriate one-letter code and amino acid number. The letters a, b, c, and d after the labels indicate to which of the four subunits the residue belongs. (A) This color representation of the crystallographic model has the C−Cα atoms and bonds colored according to the subunit in which they belong. Gold represents the C-subunit, purple the B-subunit, and dark green the D-subunit. Along with the C−Cα coloring scheme, the nitrogen atoms are in blue, oxygen atoms are in red, and carbon atoms are in gray. Note that protein atoms from three subunits, B, C, and D, are involved at the citrate position. Site B, to which L-malate and *β*-(trimethylsilyl)maleate is bound, is formed by atoms from only the B-subunit. Center to center, the two locations are about 16 Å apart with a closest approach of 12 Å. (B) This is the same as (A) except the dual images permit stereoviewing.

In the B-site, the two oxygen atoms of one carboxylate interact with the enzyme by forming hydrogen bonds to the main-chain −NH of residues 131 and 132. The oxygen atoms of the second carboxylate form hydrogen bonds with nitrogen atoms in the side chains of R126 and H129. The noncovalent distances are summarized in Table 4. The smallest distance between site A and site B is ∼12 Å. The relative location of the two sites in terms of the overall tetramer organization will be given in the Discussion section.

A few small conformational differences were observed at the B-site in the L-malate and the *β*-(trimethylsilyl)maleate structures. They are shown in Figure 6. The side chains of both N131 and D132 rotate around the $C_\alpha-C_\beta$ bond, both by nearly 90°. One of the carboxylates of the trimethylsilyl compound has moved toward D132 by nearly 1 Å, but there do not appear to be any atoms sterically forcing this movement. The other carboxylate of both L-malate and the *β*-(trimethylsilyl)maleate interacts with R126, and this salt bridge is slightly more favorable in the *β*-(trimethylsilyl)-maleate derivative. H129 also makes a small but significant rotation in toward the bound *β*-(trimethylsilyl)maleate. Finally, as is visible in Figure 6, although its electron density is less well resolved, N131 shifts away from the bound *β*-(trimethylsilyl)maleate.

The crystallographic properties and the coordination around the solvent molecule shown in Figure 4 need further discussion. The temperature factor for the water position was unusually low, around 10 $Å^2$ in the crystallographic study of the native protein. The geometry around the site was examined carefully since the electron density and nearby

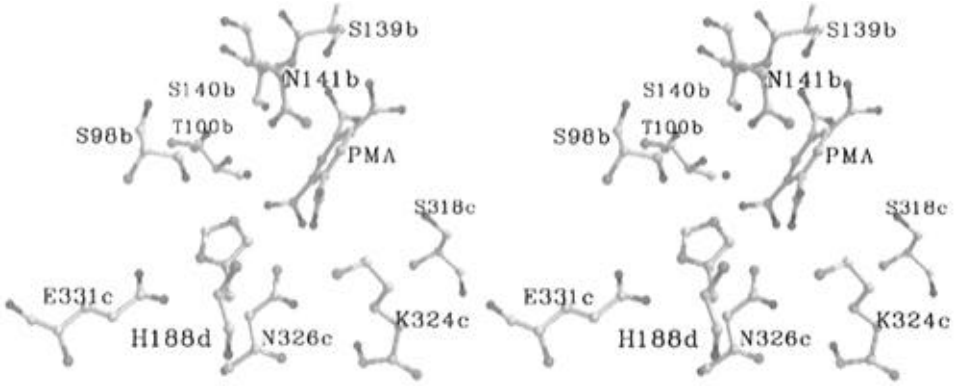

FIGURE 5: A- or active site of fumarase C with bound PMA. The stereo drawings illustrate the enzyme structure present at the A-site of fumarase as observed in the crystallographic studies of the PMA/fumarase C complex. Atoms and bonds are presented as ball and stick representations with oxygen and nitrogen atoms denoted by darkened spheres. The drawing here is taken from the crystallographic coordinates of the PMA derivative. PMA is a known competitive inhibitor of fumarase. Very similar coordination is maintained between PMA and citrate in the active site.

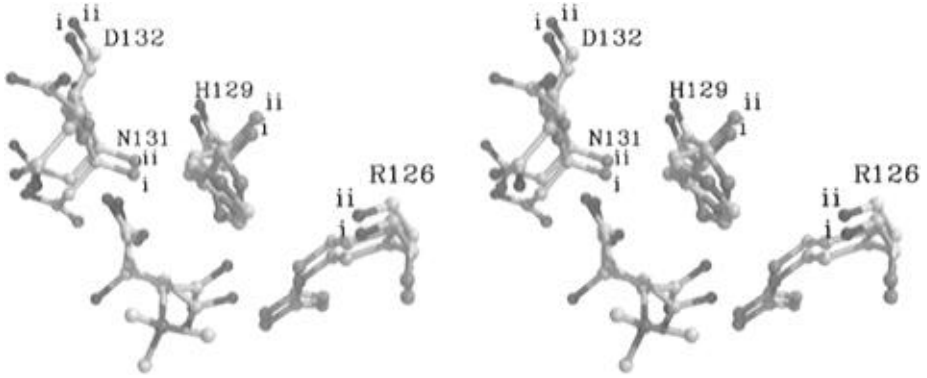

FIGURE 6: B-site in the crystal structure of fumarase C. The stereo drawings represents the atoms at the B-site in the crystal structures of native and the β-(trimethylsilyl)maleate derivative of fumarase C. Ball and stick representations are shaded as in the previous figures. Unlike the active site, binding interactions for this anion site come from only one of the three subunits. The bound structure of what is believed to be L-malate is shown as found in the native crystal structure with the β-(trimethylsilyl)maleate superimposed. The latter was obtained from the crystallographic studies of the β-(trimethylsilyl)maleate/fumarase C complex as described in the Experimental Procedures. Segments labeled with an "ii" are from the β-(trimethylsilyl)maleate structure. The only significant difference between the two complexes is the position of the side chain of D132. In the stereoview which is shown, the side chain of D32 in the β-(trimethylsilyl)maleate structure swings upward.

Table 4: Residues Participating in the B-Site of Fumarase C

side-chain atom	TMSM	distance (Å)	L-malate[a]	distance (Å)
D132-N	TMSM-O2	3.05	LMAL-O2	2.74
H129-ND1	TMSM-O4	2.77	LMAL-O4	3.03
N131-N	TMSM-O1	3.57	LMAL-O1	2.85
R126-NH1	TMSM-O3	2.88	LMAL-O3	3.11
R126-NE	TMSM-O4	2.83	LMAL-O4	2.91
R126-NH2, NH1	E7-OE2, OE1	3.42, 3.56	E7-OE1	3.51, 3.53
R126-NH2	N112-OD1	3.10	N112-OD1	3.05

[a] The distances were obtained from the crystallographic coordinates of the "native" protein but from only one of the two crystallographically independent locations.

Table 5: Distances between Active Site Water and Fumarase Side Chains

residue	distance (Å)[a]	distance (Å)[b]
H188d-NE2	2.50	2.56
S98b-OG	3.03	2.83
N141b-OD1	2.57	2.63
T100b-OG1	3.22	2.87
citrate-O1; PMA-O1	3.15	2.89
citrate-O4; PMA-O3	3.34	3.60

[a] Distances were determined using the refined crystallographic coordinates from one active site of native fumarase crystals. [b] Distances were determined using the refined crystallographic coordinates from one active site of the fumarase/PMA derivative.

atoms suggested that it may be occupied by something other than a bound water molecule. The unique coordination of the atom located at W-26 is shown in Figure 7, and the neighbor distances are given in Table 5. The ligands to W-26 are both endogenous and exogenous, and a total of six atoms are within hydrogen-bonding distance.

Although there has not been any reported metal ion requirements for fumarase activity, we were still concerned that W-26 might be something other than a water. For example, a Mg^{2+} site has been reported for the sister enzyme, aspartase; it has the effect of removing nonlinear appearances of Michaelis−Menten plots (Falzone *et al.*, 1988). To resolve the dilemma, the distances between W-26 and the nearest protein atoms were checked and are listed in Table 5. These distances fall into the hydrogen bond category rather than the semicovalent bond distances associated with metal/chelate complexes. We have therefore assigned the associated electron density at W-26 to a bound water molecule. The unusual geometry around this site suggests that the hydrogen atoms of the water molecule provide bifurcating bonds to protein atoms. The two lone pairs of the oxygen atom must also serve as hydrogen bond acceptors.

In Figure 4, there is an additional stretch of residues depicted from subunit D that forms part of domain 3 and

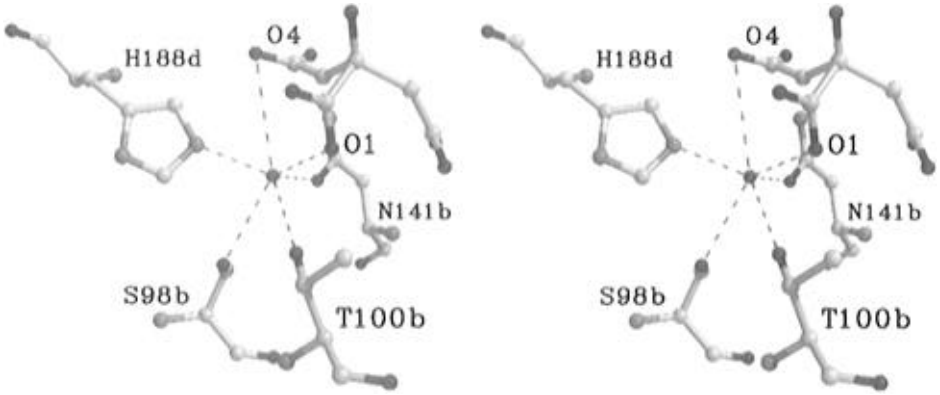

FIGURE 7: Active site water of fumarase. The stereo drawing contains the water molecule at the A-site in the native crystal structure. Atoms in this ball and stick representation are marked as in Figures 5 and 6. The water molecules is shown as a single blackened sphere. Six hydrogen-bonding coordination sites are present at or under 3.5 Å. Fumarase makes direct coordination to W-26 through H188d-NE2, N141b-OD1, S98b-OG, and T100b-OG1. Both the bound citrate and PMA in the crystal structures contribute O1 and O3 as exogenous ligands to W-26.

may be directly or indirectly involved in the catalytic activity. It also may be important to the activation site of the sister enzyme, aspartase, a supposition that will be explained in more detail in the Discussion section. Chemical modification of a single tyrosine inactivates pig heart fumarase (Beeckmans & Kanarek, 1983). Our interpretation of this result is that inactivation is due to the modification of Y418d. As is visible in Figure 4, Y418d is located near the opening of the active site depression. In aspartase, the same region of the D-subunit has also been used in fluorescence transfer experiments to measure active site distances. W430 and C140 within aspartase corresponds to A428d and S137b in fumarase, also visible in Figure 4. The distance between CB of A428d and OG of S137b is 27 Å, which is in close agreement with 22 Å calculated by energy transfer using aspartase (Murase *et al.*, 1993).

DISCUSSION

The two multicarboxylate binding sites found in the crystal structure of fumarase have very different properties. Site A is located in a relatively deep pit at the interface of three subunits while site B is in the same indentation, but nearer the molecular surface, and has contributions from a single subunit. Only the tetrameric form of fumarase is believed to be catalytically active, implying that the active site must be at a subunit/subunit interface (Kanarek *et al.*, 1964). Furthermore, the three different subunit segments contributing to site A are the highly conserved segments in the family homology table. Hence, the initial circumstantial evidence pointed to site A as the active site.

There are several more observations that provide further support for site A being the active site. All mutational studies have indicated that specific residues within the A-site are directly connected to enzymatic activity. Mutations at K324 in aspartase and E315 in human fumarase have knocked out activity in both enzymes (Sarbus *et al.*, 1994; Bourgeron *et al.*, 1994). A H129N mutant in site B generated in our laboratory has little or no effect on catalytic activity. If H129 were to be part of the acid/base pair utilized during the reaction mechanism, the mutation to asparagine should have produced a measurable change in catalytic activity. In addition, the lack of conservation among 22 proteins of the fumarase family of residues R126 through D132 suggests that the B-site is not involved in the catalytic reaction. In fact, excluding fumarase and aspartase, none of the other family members including arginosuccinate lyase, adenylosuccinate lyase, 3-carboxy-*cis*,*cis*-muconate lactonizing enzyme, and δ-crystallin even have this stretch of residues. Finally, the presence of the well-characterized competitive inhibitor, PMA, confirms the selection of site A as the active site.

The active site, as observed in these three crystal structures, allows for the definition of two important issues for the fumarase family of enzymes: (1) interactions necessary for binding the substrate(s), and (2) groups which may participate in the catalytic reaction, for example, the bases B1 and B2 in Figure 1, and the role of the catalytic water, W-26. Table 3 provided a summary of the distances between the various ligand atoms and side chains at the active site. Subunit B is especially important as it donates residues to both the active site and the B-site. At the active site, side chains from S98, T100, S139, S140, and N141 of subunit B interact with the competitive inhibitors. Subunit C provides K324, N326, and E331, and subunit D donates T187 and H188. These active site components come from three subunits but are held in a relatively rigid place by the network of polar interactions listed in Table 6.

From the inhibitor locations, it appears that the enzyme/substrate interactions occur mainly through the carboxylate moiety. However, PMA has four, citrate has three, and the true substrates L-malate or fumarate have two carboxylate groups. In the crystal structures, two carboxylates from the citrate and PMA are essentially superimposable as seen by comparing Figures 4 and 5. We have selected these two positions as representing those which would most likely occur within the L-malate/fumarate enzyme complex.

The side chains of N326, K324, T187, and H188 appear to form a network of hydrogen bonds and essentially encircle the carboxylate of citrate which we propose would be at the C4 position in L-malate. It is this location which would have to accommodate any *aci*-carboxylate intermediate. K324 and N326 are in a region of positive potential in the active site that might be utilized to help to stabilize the highly charged *aci*-carboxylate intermediate. In an alignment containing 22 fumarase family members K324 and N326 are two of the invariant residues.

Of the remaining two carboxylate moieties of the bound citrate, a second is again nearly superimposable with a

carboxylate from PMA. It has been designated as the approximate position of the C1 carboxylate of either substrate, L-malate or fumarate. This location also interacts with the side chain of N326. In addition, hydrogen bonds are formed with the side chain of T100. Although we fitted an L-malate model into the active site on the basis of the location of these two carboxylate moieties, there are enough degrees of freedom that it is difficult to predict the precise location of this end of the substrate.

In spite of the similarities in coordination of citrate and PMA at the active site, Table 3 also shows that subtle differences exist. In the case of citrate and PMA, the third carboxylate forms hydrogen bonds with two serine side chains. The OG atoms from S139 and S140 form hydrogen bonds to two different oxygen atoms of this carboxylate, locking it into position. In addition, the next residue, N141, is also relatively close.

The fourth carboxylate of PMA interacts with the side-chain atoms of N131 and N135 on the π-helix. Since the peptide nitrogen of N131 also interacts with the carboxylate of ligands bound to the B-site, this asparagine serves as a link between the two sites. Although it is unclear what effect this linkage might have on enzyme activity, the catalytic site is clearly connected by an intricate network of hydrogen bonds to the B-site, and this connection involves the one-turn π-helix from residues H129 to N135.

An intricate part of the active site for fumarase is a water molecule, W-26. It has a temperature factor between 10 (citrate/fumarase) and 18 Å^2 (PMA/fumarase) and has essentially the same interactions in both crystalline complexes. The unique coordination tabulated in Table 5 may be responsible for its crystallographic stability. This active site water is held in place by polar groups from both the protein and the bound ligand. With respect to the latter, W-26 is positioned between the C1 and C4 positions of both the bound citrate and PMA ions, allowing for hydrogen bonds to O1 and O3. W-26 is within hydrogen-bonding distance of S98, T100, N141, and H188. The atom NE2 from H188d forms a particularly short, 2.4 Å, hydrogen bond in the citrate crystal structure.

In terms of potential reaction mechanisms, the crystallographic studies point to several important features. First, fumarase crystals have been soaked with analogs of both fumarate and L-malate, and neither had any effect on the crystalline state. This suggests that the conformational changes required to differentiate between the fumarate and L-malate forms of the enzyme are small, perhaps inconsequential. Even though fumarase has no activity under the crystallization conditions, this is accounted for by the known competitive inhibition by citrate or PMA.

We have used the inhibitor sites to suggest the identity of the two basic groups labeled B_1 and B_2 in Figure 1. In the direction of fumarate production, B_1 must be able to remove a methylene proton from the carbon atom at the C3 position of L-malate. Providing that the orientation of the L-malate has been modeled correctly in the crystal structures, the closest atom to this position is the active site water molecule. The very short hydrogen bond to H188 may be a mechanism for introducing negative charge on the water. As is also shown in Figure 1, removal of the methylene proton introduces an extra negative charge, forming the so-called *aci*-carboxylate intermediate. The positive potential generated by K324c may be used to stabilize this intermediate.

Perhaps the short hydrogen bond between H188d and W-26 in both enzyme complexes is in fact similar to the proposed low-barrier hydrogen bond thought to exist in fumarase and shown in other enzymes (Cleland, 1992). Short hydrogen bonds have been theorized to have low energy barriers for hydrogen or proton movement. They are believed to occur when steric factors force similarities in the p*K*'s of the two groups. In some instances, they may be able to promote proton movement in appropriate enzymatic reactions (Cleland, 1994). In this case, the proposed low barrier bond would be used to activate water which then would be involved in the removal of the methylene hydrogen at the C3 position of L-malate.

The hypothetical chain of events would include the E331−H188 charge-relay pair found in fumarase. This in turn would affect the basicity of H188. H188 would then "activate" the water. The altered water molecule would be utilized to remove the proton at the C3 position of L-malate and form the unstable carbanion. During the catalytic reaction, it has been hypothesized that it is necessary to lower the pK_a of the proton from ~30 down 23 pH units to match the pK_a of the base on the enzyme at ~5.7 (Cleland & Kreevoy, 1994). A parallel alternative is to raise the p*K* of the attacking base to near that of the methylene hydrogen. This would account for the short hydrogen bond between H188 and the active site water.

The protonated form of K324 might serve two purposes. First, it could help to stabilize the *aci*-carboxylate intermediate. This might be facilitated by the presence of the now protonated H188. Second, K324 could be responsible for the removal of the OH^- from the substrate with the formation of a water molecule. In the crystal structures, minor changes in the χ values of the K324 side chain would bring the ϵ-amino group of K324 very close to the −OH of L-malate. We are proposing that it is the functional group shown as B_2 in Figure 1.

The proton produced when L-malate is converted into fumarate would probably have to travel through the W26−H188−E331 route to equilibrate with water in the milieu. The proton at the C3 position removed in this fashion would then match the description of the sticky proton shown to be the last product off the enzyme during the catalytic cycle (Hansen *et al.*, 1969; Rose *et al.*, 1992). Along with critical hydrogen bonds to the inhibitors, the residues within the three-subunit active site form a network of hydrogen bonds between segments of polypeptide chain and some between subunits. This series of hydrogen bonds is listed in Table 6; they most likely add rigidity to the multisubunit active site.

Intersubunit interactions described in Table 6 include H188, K324, T187, E315, and E331. In one instance, the importance of these interactions is borne out by a genetically transferred mutation. A severe deficiency in fumarase activity, less than 0.5% of normal, has been found in siblings born to parents with the mutated gene. The clinical features in early fumarase deficiency involve neurological impairment and encephalopathy (Bourgeron *et al.*, 1994). Utilizing the *E. coli* sequence, this mutation corresponds to E315, which is within one of the three highly conserved regions in the fumarase superfamily. In the crystal structure, E315 makes a hydrogen bond with T328 which is about 8 Å from the inhibitor/active site.

Table 6: Hydrogen-Bonding Interactions between Side Chains at the Active Site

side-chain donor	side-chain acceptor	distance (Å)[a]	distance (Å)[b]
H188D-ND1	E331C- OE1, OE2	2.76, 3.32	2.75, 3.28
K324C-NZ	N326C-OD1	3.02	2.95
K324C-NZ	T187D-OG1	3.10	3.27
T100B-OG1	S98B-OG	2.74	2.81
S98B-OG	T96B-OG1	3.50	3.43
T328C-OG1	E315C-OE1	2.74	2.86

[a] Distances were determined using the refined crystallographic coordinates from native fumarase crystals. [b] Distances were determined using the refined crystallographic coordinates from the fumarase/PMA derivative. Hydrogen bond distances were determined for only one of the two crystallographically independent sites.

The role of the B-site in the interconversion of L-malate and fumarate is unclear. The relative location of the A- and B-sites is visible in Figure 4. The closest distance between the two sites is 12 Å. In the native structure, site B appeared to have electron density resembling that of the native substrate L-malate. In the β-(trimethylsilyl)maleate derivative, the additional trimethylsilyl group was clearly visible in the electron density.

How did L-malate get into site B in the native crystals? The native X-ray data were collected using crystals grown from a high concentration of citrate buffer and poly(ethylene glycol) 4000. L-Malate could have come from the purification protocol when it was used to elute fumarase C from the pyromellitic acid affinity column. Nonetheless, the electron density now assigned to L-malate and shown in Figure 4 was missed in the first reported structure (Weaver *et al.*, 1995).

We have checked the enzymatic activity of fumarase in the presence of the crystallization buffer, and it is fully inhibited. The inhibition has been verified with three different substrates: L-malate, fumarate, and β-(trimethylsilyl)maleate. On the basis of these data, we feel confident that citrate binds at the active or A-site, and it has little affinity, if any, for the B-site. Furthermore, the only side chain in site B that could act as a base for proton removal during a catalytic cycle is H129. H129 was replaced with an asparagine, and the resulting enzyme had activity comparable to that of the wild-type enzyme (Weaver, Lees, and Banaszak, unpublished results).

The biochemical purpose of the B-site cannot be determined with the crystallographic data. Kinetic studies of the related aspartase reaction indicated that it is markedly activated by the product L-aspartate (Ida & Tokushige, 1985; Karsten *et al.*, 1986). Using fluorescence energy transfer measurements and aspartase, the activator site is estimated to be about 10−12 Å from the active site (Murase *et al.*, 1993). The relative distance agrees well with separation of the A-site and B-site in the fumarase maps.

The steric interrelationship between the two sites has been analyzed, and the residues involved in coordinating the L-malate and β-(trimethylsilyl)maleate at site B were listed in Table 4. They include hydrogen bonds with the side-chain atoms from R126 and the backbone nitrogen atoms from N131 and D132. The backbone nitrogen atoms for N131 and D132 are at the beginning of a π-helix, and the position of O1 and O2 from each ligand appears to be ideally suited for a pair of hydrogen bonds. H129 also forms a hydrogen bond to the O4 atom of both site B ligands.

While it is tempting to assume that site B is an activation site homologous with that described above for aspartase, it is difficult to directly involve atoms in this location with those in the catalytic center. At best, it appears that a ligand in place at site B could have some subtle electrostatic effect, changing the properties of side chains involved in catalysis. A second possibility is that, by reducing access to the active site pit, it facilitates the fumarate to L-malate interconversion. Work is now in progress on studying site-directed mutants at both the active site, site A, and site B.

CONCLUSIONS

In general, the crystals of fumarase and its active site derivatives produce high quality X-ray diffraction data to high resolution which refined to acceptable *R*-factors. The discovery of two adjacent binding sites for carboxylic acids on fumarase has been interpreted as an active site, site A, and an activation site, site B. The active site is located in a deep pit on the surface and contains an especially tightly bound water molecule which is highly coordinated. The interactions between this active site water and fumarase include a short hydrogen bond to H188. In addition, side chains located at the active site belong to three subunits in the tetramer. On the basis only of the stereochemistry, we propose that it is a water molecule that is involved in the first step of the catalytic reaction—the removal of a hydrogen ion from a methylene carbon. The presumed intermediate is an *aci*-carboxylate compound which we suggest could be stabilized by K324. This lysine side chain would also be involved in supplying a proton for the formation of a water molecule resulting from the removal of an −OH from the L-malate substrate.

ACKNOWLEDGMENT

We thank Ed Hoeffner for the maintenance of both the X-ray and computational resources in the Dietrich Structural Biology Laboratory at the University of Minnesota and Sherry Sahr, who has repeatedly helped with proofreading. We acknowledge the support for computing resources from the Minnesota Supercomputer Institute. The authors would like to thank Professor Cleland at the University of Wisconsin and Dr. E. Rose from the Institute of Cancer Research, Fox Chase, PA, for helpful discussions regarding the fumarase mechanism based on their own studies and their familiarity with the biochemical literature. Professor Cleland also supplied us with a halogenated fumarate compound, 3-nitro-2-hydroxypropionate. This did not bind at the lower pH's used to prepare crystals. Thanks also goes out to Dr. Y. Apeloig at the Israel Institute of Technology for providing samples of β-(trimethylsilyl)maleate which were used in the crystal studies.

REFERENCES

Alberty, R. A., & Bock, R. M. (1953) *Proc. Natl. Acad. Sci. U.S.A. 39*, 895−900.

Alberty, R. A., Massey, V., Frieden, C., & Fuhlbrigge, A. R. (1954) *J. Am. Chem. Soc. 76*, 2485.

Beeckmans, S., & Kanarek, L. (1983) *Biochim. Biophys. Acta 743*, 370−378.

Biton, R. (1994) Research Thesis, I−IV and p 87, Department of Chemistry, Technion-Israel, Haifa, Israel 32000.

Blanchard, J. S., & Cleland, W. W. (1980) *Biochemistry 19*, 4506−4513.

Bourgeron, T., Chretien, D., Poggi-Bach, J., Doonan, S., Rabier, S., Letouzé, P., Munnich, A., Rötig, A., Landrieu, P., & Rustin, P. (1994) *J. Clin. Invest. 93*, 2514−2518.
Brandt, D., Barnett, L., & Alberty, R. (1963) *J. Am. Chem. Soc.* 85, 2204−2209.
Brünger, A. T., Kuriyan, J., & Karplus, M. (1987) *Science 235*, 458−460.
Cleland, W. W. (1992) *Biochemistry 31*, 317−319.
Cleland, W. W., & Kreevoy, M. M. (1994) *Science 264*, 1887−1890.
Conway, A., & Koshland, D. E. (1968) *Biochemistry 7*, 4011−4022.
Falzone, C. J., Karsten, W. E., Conly, J. D., & Viola, R. E. (1988) *Biochemistry 27*, 9089−9093.
Ferrin, T. E., Huang, C. C., Jarvis, L. E., & Langridge, R. (1988) *J. Mol. Graphics 6*, 13−27.
Greenberg, J. T., Monach, P., Chou, J. H., Josephy, P. D., & Demple, B. (1990) *Proc. Natl. Acad. Sci. U.S.A. 87*, 6181−6185.
Greenhut, J., Umezawa, H., & Rudolph, F. B. (1985) *J. Biol. Chem. 260*, 6684−6686.
Guest, J. R., Miles, J. S., Roberts, R. E., & Woods, S. A. (1985) *J. Gen. Microbiol. 131*, 2971−2984.
Hansen, J. N., Dinovo, E. C., & Boyer, P. D. (1969) *J. Biol. Chem. 244*, 6270−6279.
Hill, R. L., & Teipel, J. W. (1971) *Enzymes 5*, 539−571.
Howard, A. J., Gilliland, G. L., Finzel, B. C., Poulos, T. L., Ohlendorf, D. H., & Salemme, F. R. (1987) *J. Appl. Cryst. 20*, 383−387.
Ida, N., & Tokushige, M. (1985) *J. Biochem. 98*, 35−39.
Jones, T. A., Zou, J. Y., Cowan, S. W., & Kjeldgaard, M. (1991) *Acta Crystallogr. A47*, 110−119.
Kanarek, L., Marler, E., Bradshaw, R. A., Fellows, R. E., & Hill, R. L. (1964) *J. Biol. Chem. 239*, 4207−4211.
Karsten, W. E., Gates, R. B., & Viola, R. E. (1986) *Biochemistry 25*, 1299−1303.
Keruchenko, J. S., Keruchenko, I. D., Gladilin, K. L., Zaitsev, V. N., & Chirgadze, N. Y. (1992) *Biochim. Biophys. Acta 1122*, 85−92.
Laskowski, R. A., MacArthur, M. W. Moss, D. S., & Thornton, J. M. (1993) *J. Appl. Crystallogr. 26*, 283−291.
Liochev, S., & Fridovich, I. (1992) *Proc. Natl. Acad. Sci. U.S.A. 89*, 5892−5896.
Murase, S., Kawata, Y., & Yumoto, N. (1993) *Biochem. Biophys. Res. Commun. 195*, 1159−1164.
Porter, D. J. T., & Bright, H. J. (1980) *J. Biol. Chem. 255*, 4772−4780.
Rebholz, K. L., & Northrop, D. B. (1994) *Arch. Biochem. Biophys. 12*, 227−233.
Rose, I. A., Warms, J. V., & Kuo, D. J. (1992) *Biochemistry 31*, 9993−9999.
Rose, I. A., Warms, J. V., & Yuan, R. G. (1993) *Biochemistry 32*, 8504−8511.
Sarbus, A. S., Schindler, J. F., & Viola, R. E. (1994) *J. Biol. Chem. 269*, 6313−6319.
Simpson, A., Bateman, O., Driessen, H., Lindley, P., Moss, D., Mylvaganam, S., Narebor, E., & Slingsby, C. (1994) *Nat. Struct. Biol. 1*, 724−733.
Weaver, T. M., Levitt, D. G., & Banaszak, L. J. (1993) *J. Mol. Biol. 231*, 141−144.
Weaver, T. M., Levitt, D. G., Donnelly, M. I., Wilkens-Stevens, P. P., & Banaszak, L. J. (1995) *Nat. Struct. Biol. 2*, 654−662.
Woods, S. A., Miles, J. S., Roberts, R. E., & Guest, J. R. (1986) *Biochem. J. 237*, 547−557.
Woods, S. A., Schwartzbach, S. D., & Guest, J. R. (1988) *Biochim. Biophys. Acta 954*, 14−26.

BI9614702